Eur. Phys. J. A **22**, 61–67 (2004)
DOI 10.1140/epja/i2004-10013-1

THE EUROPEAN PHYSICAL JOURNAL A

Neutron transition densities for the 2^+–8^+ multiplet of states in ^{90}Zr

M.S. Onegin[1,a] and A.V. Plavko[2,b]

[1] Theory Division, Petersburg Nuclear Physics Institute, 188350 Gatchina, Leningrad district, Russia
[2] State Polytechnic University of St. Petersburg, 194223 Thorez Prospekt, 40-3-9, St. Petersburg, Russia

Received: 9 January 2004 / Revised version: 4 April 2004 /
Published online: 14 September 2004 –
Communicated by J. Äystö

Abstract. Neutron transition densities for the 2^+–8^+ levels in ^{90}Zr were extracted in the process of analyzing $(\mathbf{p}, \mathrm{p}')$ scattering at 400 MeV. They were compared with the calculated neutron transition densities and with the experimental proton transition densities. Radial distributions of the experimental neutron and proton transition densities for each state were found to be different.

PACS. 25.40.Ep Inelastic proton scattering – 21.10.-k Properties of nuclei; nuclear energy levels

1 Introduction

The nuclear structure of the 2^+–8^+ multiplet of levels of ^{90}Zr can be described by a simple configuration in the framework of the shell model [1]. In this paper it was demonstrated that the levels position of this nucleus can be reproduced by taking into account proton shells only. The g-factor measured for the 2_1^+ level is also consistent with a dominant $g_{9/2}$ proton configuration and a closed $N = 50$ neutron shell [2]. At the same time the measured $B(EL)$ and charged transition densities for the multiplet of levels point to a considerable core polarization admixture to them. The analysis of inelastic proton scattering with the excitation of these levels can give information about the neutron shell contribution. It has been analyzed in various publications (see [3–5] and references therein for earlier papers). In these works, the authors tried to describe experimental data by the shell model procedure with a limited basis size or by the collective model of inelastic excitation. The lack of the necessary transition strength in the microscopic calculations based on a simple $(\pi 1g_{9/2})^2$ configuration made them introduce enhancement factors needed to adjust the calculated cross-sections to experimental ones.

In the present paper, we employ a semi-microscopic approach in which only the matter component of transition densities is used to describe the cross-section and analyzing power of inelastic scattering. Earlier [6–8] it was demonstrated that this approach was adequate for the description of inelastic scattering at medium and intermediate energies for low-lying states with a large admixture of a core polarization component in their nuclear wave functions. Since the proton transition density can be determined independently in an electron scattering experiment, proton scattering can be used to obtain the second component of the matter density —the experimental neutron transition density. Our analysis is based on the empirical effective interaction of Kelly [9]. The Kelly forces were tested in the analysis of inelastic proton scattering by nuclei with $N = Z$. In this case the neutron transition densities extracted in the description of experimental observables coincide within errors with the proton transition density [7]. In this paper, we use the experimental data of [5] to deduce these important characteristics of nuclear excitation for the multiplet of the 2_1^+, 4_1^+, 6_1^+, 8_1^+ levels in ^{90}Zr. Earlier a slightly similar procedure was undertaken to deduce the model-dependent neutron transition density. It was done for the first member of this multiplet only (2^+). The result will be examined in our paper further on.

2 Calculation scheme

In our study of proton scattering, we have used the calculation scheme provided by the linear expansion analysis (LEA) code from Kelly [10]. Our calculations have been performed in the DWIA framework. The same density-dependent empirical interaction developed by J.J. Kelly *et al.* is used in the calculations of the optical potential and transition potential for inelastic scattering in the folding model formalism. The density dependence of the isoscalar part of the t-matrix was parametrized in the following

[a] e-mail: onegin@thd.pnpi.spb.ru
[b] e-mail: rodimkina@hotbox.ru

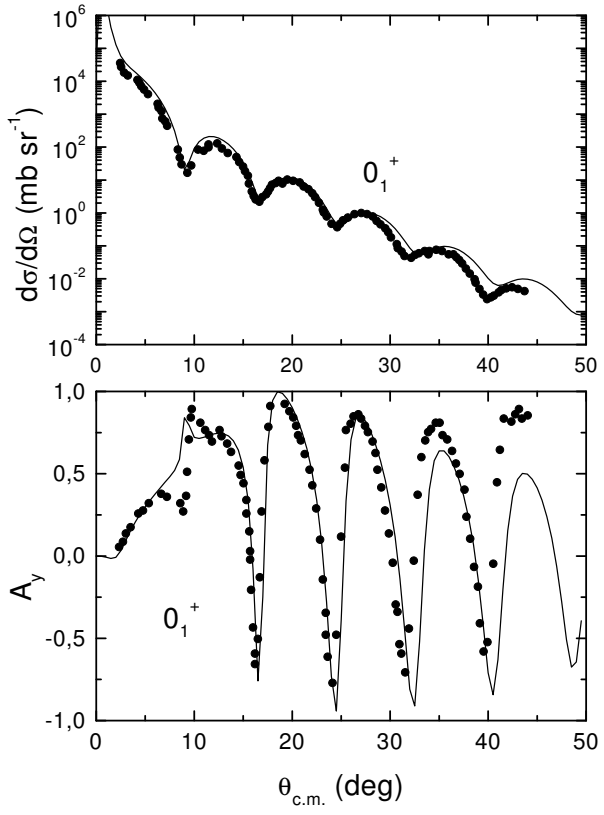

Fig. 1. Elastic cross-section and analyzing power for proton scattering from ^{90}Zr at 400 MeV. The circles are the data from ref. [5]. The curves are microscopical folding model calculations.

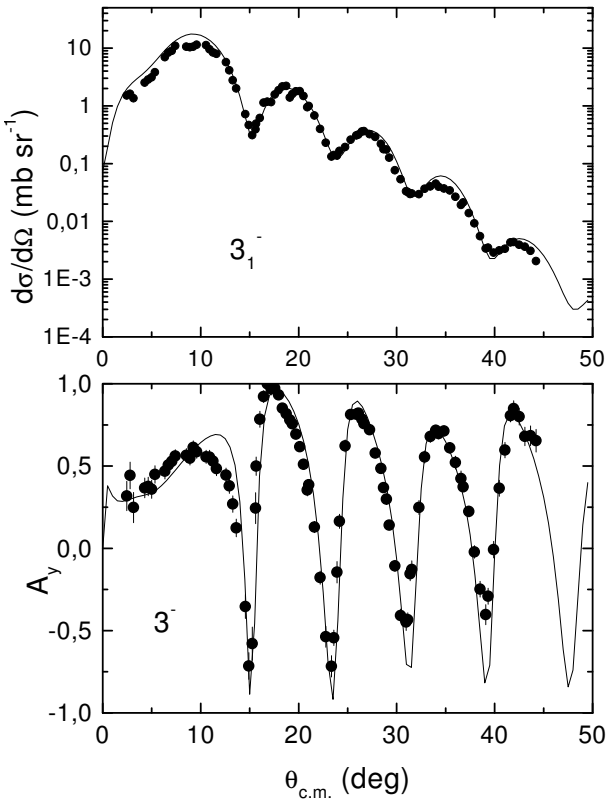

Fig. 2. Inelastic cross-sections and analyzing power for proton scattering from ^{90}Zr at 400 MeV for the 3_1^- level. The circles are the data from refs. [16,17]. The curves are microscopical folding model calculations.

form:

$$\begin{aligned}
\operatorname{Re} t^C(q,\kappa) &= S_1 \operatorname{Re} t^C(q,0) + b_1\kappa^3\left[1+(q/\mu_1)^2\right]^{-1},\\
\operatorname{Im} t^C(q,\kappa) &= \left(S_2 - d_2\kappa^2\right)\operatorname{Im} t^C(q,0),\\
\operatorname{Re}\tau^{LS}(q,\kappa) &= S_3 \operatorname{Re}\tau^{LS}(q,0) + b_3\kappa^3\left[1+(q/\mu_3)^2\right]^{-2},\\
\operatorname{Im}\tau^{LS}(q,\kappa) &= S_4 \operatorname{Im}\tau^{LS}(q,0) + b_4\kappa^3\left[1+(q/\mu_4)^2\right]^{-2},
\end{aligned}$$

where $\kappa = k_{\mathrm{F}}/1.33$. The parameters S_1, b_1, S_2, d_2, S_3, b_3 were obtained in an adequate description of inelastic scattering from different nuclei. The density dependence of $\operatorname{Im}\tau^{LS}$ reproduces one of the Ray effective interactions: $S_4 = 1.0$, $b_4 = -1.92\,\mathrm{MeV\,fm^5}$ [11,12]. The mass parameters have the values $\mu_1 = 2.0\,\mathrm{fm}^{-1}$, $\mu_3 = 6.0\,\mathrm{fm}^{-1}$ and $\mu_4 = 1.0\,\mathrm{fm}^{-1}$. As a density-independent interaction in the evaluation of these equations, we use the Franey-Love t-matrix [13]. We did not take into account the density dependence of the isovector part of the interaction in this work. As a first approximation, this is justified by the fact that the isovector part of free NN t-matrix at this energy is more than four times smaller than the isoscalar one [14]. The parameters of the effective interaction used in this paper are presented in table 1. They were obtained in the description of proton inelastic scattering from ^{16}O and ^{40}Ca [12,15] at 318 MeV. These potentials are folded with the nucleon densities of the ground state [18] and with the transition densities of the excited states, respectively. We employ a zero-range approximation for the exchange and use the local density approximation based upon the density at the projectile position in the analysis of a 400 MeV proton scattering experiment.

Table 1. Parameters of empirical effective interaction of Kelly [12,15].

S_1	b_1 (MeV fm^3)	S_2	d_2	S_3	b_3 (MeV fm^5)
1.070	142.2	1.001	−0.042	0.781	5.88

The analysis of inelastic scattering with the excitation of the 3_1^- level serves for us as an additional test of the NN forces we used. We consider this excitation as pure isoscalar (neutron transition density has been taken to be equal to proton transition density). This excitation is collective in nature ($B(E3) = 26 \pm 3$ W.u.). That is why for its description we can use the QRPA theory. The calculations performed within the framework of this theory confirm the isoscalar nature of this excitation [19]. The point-proton density for the 3_1^- level obtained in inelastic electron scattering [20] was taken from the work [21].

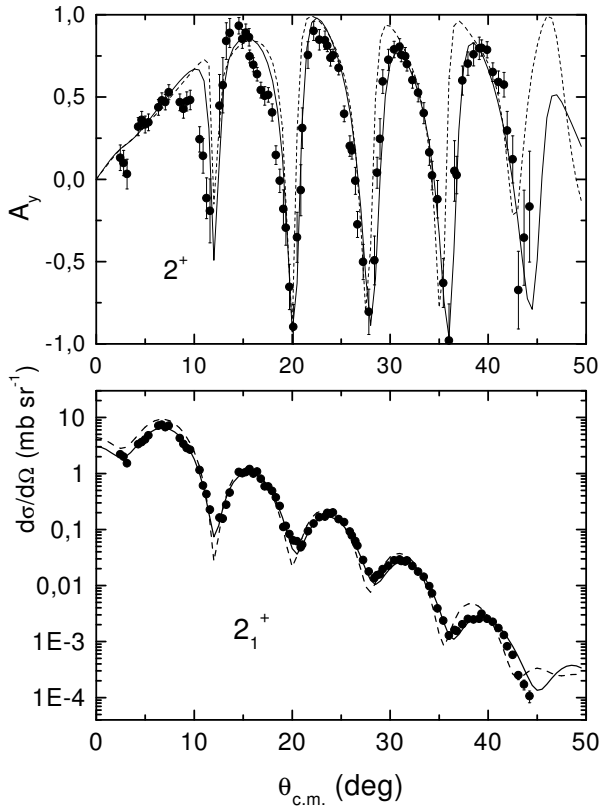

Fig. 3. Differential inelastic cross-section and analyzing power for proton inelastic scattering to the 2_1^+ state in ^{90}Zr at 400 MeV. The circles are the data from refs. [5,17]. The curves are microscopical folding model calculations. The dashed curves: isoscalar option for transition densities; the full curves: empirical fitted neutron transition density.

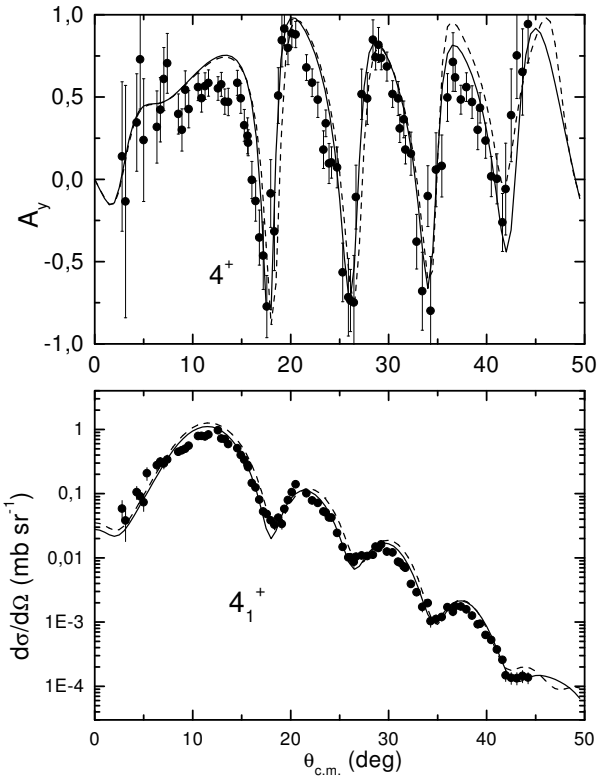

Fig. 4. Inelastic cross-sections and analyzing power for proton scattering from ^{90}Zr at 400 MeV. The 4_1^+ level. The circles are the data from refs. [5,17]. The curves are microscopical folding model calculations. The dashed curves: isoscalar option for transition densities; the full curves: empirical fitted neutron transition density.

Calculations were performed in folding formalism in the same manner as for the 2_1^+–8_1^+ levels. The comparison of the calculated cross-sections of the elastic and inelastic 3_1^- exitation and their analyzing powers with the experimental data is presented in figs. 1, 2. The overall agreement is satisfactory. Therefore, we can be confident of the adequate use of the NN t-matrix interaction and folding procedure at the given energy. For the description of inelastic excitations only matter transition densities are used in the folding procedure to obtain scattering potentials. The proton transition densities have been obtained by unfolding the proton charge densities from the charge transition densities extracted in inelastic electron scattering [20]. According to [10], neutron transition densities $\rho_{\rm tr}^{\rm n}$ for the transition of multipolarity L have been parametrized using the Laguerre-Gaussian expansion (LGE)

$$\rho_{{\rm tr},L}^{\rm n}(r) = \sum_{\nu} a_\nu x^L e^{-x^2} L_\nu^k\big(2x^2\big), \qquad (1)$$

where $k = L + \frac{1}{2}$ and $x = r/b$. The fitting procedure is similar to that employed in [22] for the ^{88}Sr nucleus. The oscillator parameter b has been set to 2.2 fm. L_ν^k is a generalized Laguerre polynomial of order ν. The unknown coefficients a_ν have been obtained by fitting the calculated differential cross-sections for the nuclear levels in question to the experimental data of [5,17]. The analysis includes a high-q bias and an estimate of the incompleteness error that results from the limitation of the data to the finite momentum transfer. A tail bias is used to damp unphysical oscillations of the density for $r \geq r_{\rm m}$, where it is assumed that $\rho \propto e^{-dr}$ is beyond the match radius $r_{\rm m} = 6.5$ fm. The parameter d is adjusted to the fitted density at the match radius $r_{\rm m}$.

3 Results of culculations

The fits to the cross-section and analyzing power data are displayed in figs. 3, 4, 5, 6. The LGE expansion coefficients for the neutron transition densities in question are tabulated in table 2. The fitted neutron transition densities presented in fig. 7 are compared with the proton transition densities for the same levels. In figs. 3, 4, 5, 6 the dashed curve also represents the calculated cross-sections and the analyzing power in the approximation of a pure-isoscalar

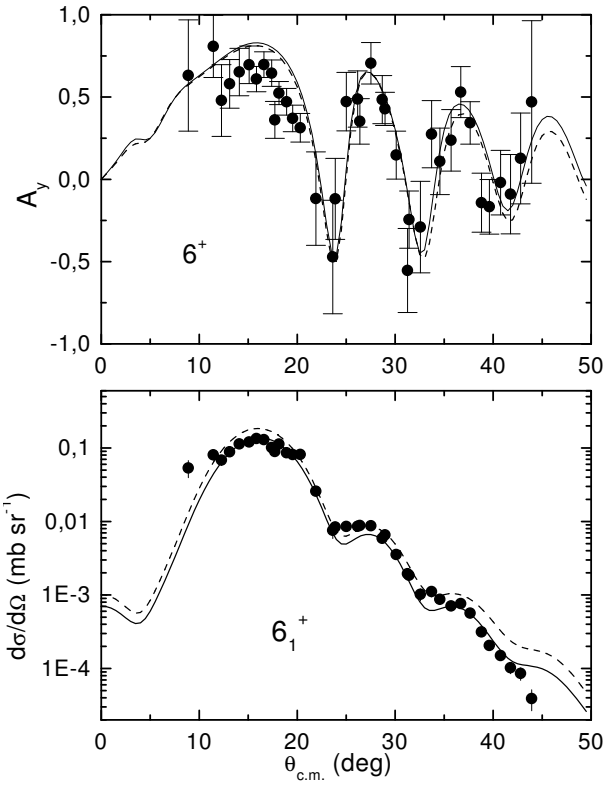

Fig. 5. Inelastic cross-sections and analyzing power for proton scattering from ^{90}Zr at 400 MeV. The 6^+_1 level. The circles are the data from refs. [5,17]. The curves are microscopical folding model calculations. The dashed curves: isoscalar option for transition densities; the full curves: empirical fitted neutron transition density.

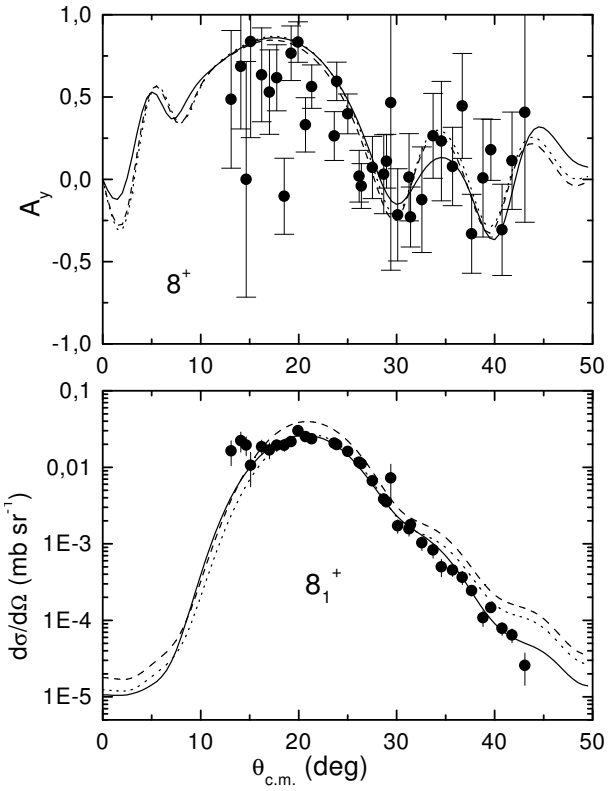

Fig. 6. Inelastic cross-sections and analyzing power for proton scattering from ^{90}Zr at 400 MeV. The 8^+_1 level. The circles are the data from refs. [5,17]. The curves are microscopical folding model calculations. The dashed curves: isoscalar option for transition densities; the full curves: empirical fitted neutron transition density; the dotted curves: scaled proton transition density.

Table 2. Neutron transition densities expansion coefficients a_ν for ^{90}Zr expressed in units fm^{-3}.

ν	2^+_1	4^+_1
1	$(-3.46 \pm 1.59) \times 10^{-3}$	$(3.25 \pm 0.61) \times 10^{-3}$
2	$(-9.32 \pm 0.65) \times 10^{-3}$	$(-2.50 \pm 0.19) \times 10^{-3}$
3	$(8.02 \pm 0.27) \times 10^{-3}$	$(7.82 \pm 0.69) \times 10^{-4}$
4	$(-3.02 \pm 1.33) \times 10^{-4}$	$(1.39 \pm 0.24) \times 10^{-4}$
5	$(-3.66 \pm 0.58) \times 10^{-4}$	$(-1.92 \pm 0.93) \times 10^{-5}$
6	$(-1.48 \pm 1.95) \times 10^{-5}$	$(-8.15 \pm 1.80) \times 10^{-6}$
ν	6^+_1	8^+_1
1	$(9.45 \pm 0.61) \times 10^{-4}$	$(1.27 \pm 0.09) \times 10^{-4}$
2	$(-1.36 \pm 0.17) \times 10^{-4}$	$(6.90 \pm 3.68) \times 10^{-6}$
3	$(9.01 \pm 4.14) \times 10^{-6}$	$(6.12 \pm 1.37) \times 10^{-6}$
4	$(3.27 \pm 2.37) \times 10^{-6}$	$(7.78 \pm 2.61) \times 10^{-7}$
5	$(-1.64 \pm 0.70) \times 10^{-6}$	$(1.35 \pm 1.00) \times 10^{-7}$
6	$(-1.53 \pm 0.19) \times 10^{-6}$	$(-1.98 \pm 0.40) \times 10^{-7}$

character of the excitations. It can be seen there from the comparison with the experiment that this approximation is unacceptable.

The transition strength is customarily characterised by the moment

$$M_\lambda = \int \mathrm{d}r r^{L+2} \rho^\lambda_L(r), \tag{2}$$

where $\lambda = (\mathrm{p}, \mathrm{n})$ for protons and neutrons, respectively, and $\rho^\lambda_L(r)$ is the radial dependence of the corresponding transition density. We use the following normalization of the proton transition density:

$$B(EL) \uparrow = (2L+1) M^2_\mathrm{p}, \tag{3}$$

where $B(EL) \uparrow$ is the reduced electromagnetic transition probability for the level of multipolarity L. The values of the transition matrix elements ratio $M_\mathrm{n}/M_\mathrm{p}$ can serve as an integral measure of the neutron shells contribution to the inelastic transitions in question. The M_λ value is highly sensitive to the tail bias of the radial density distribution. The latter, in its turn, is determined by small-momentum-transfer experimental data for the transition analyzed. Unfortunately, there is a lack of such data for the 6^+ and especially for the 8^+ states [5,17]. Therefore, the extracted neutron transition densities may be inaccurate

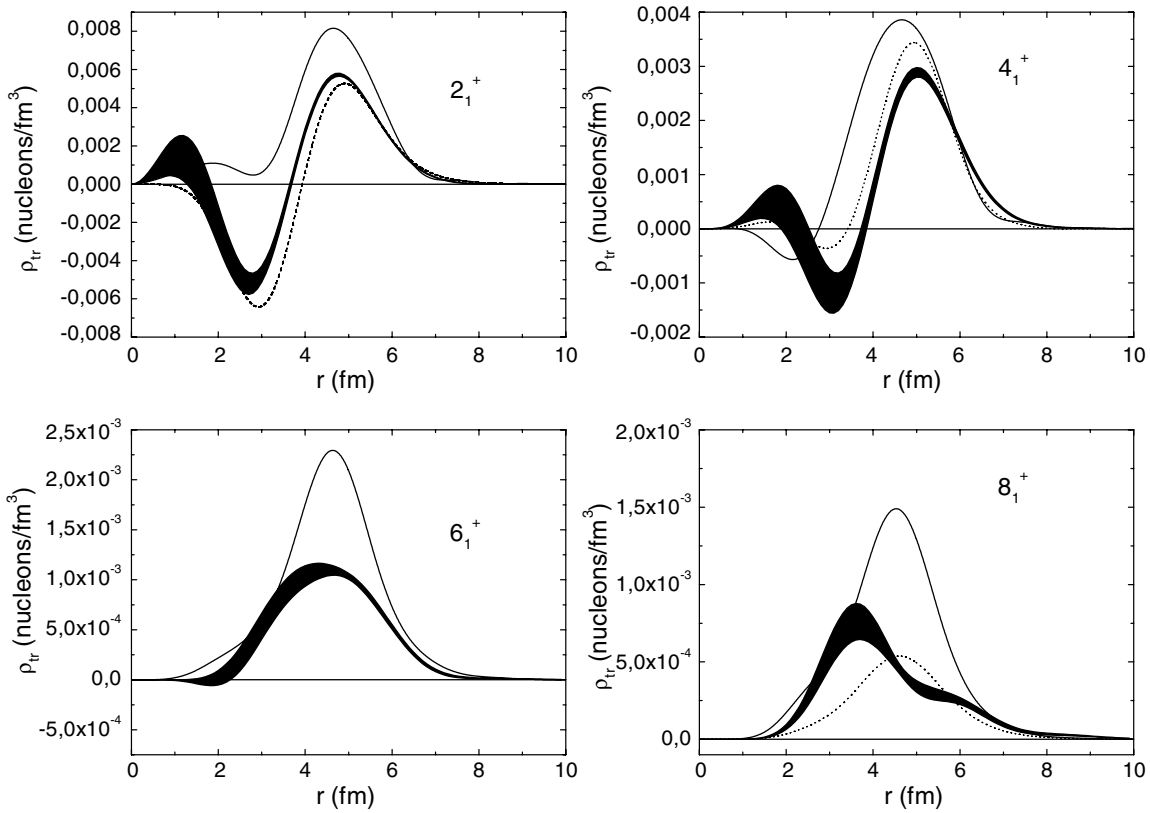

Fig. 7. The experimental neutron transition densities for the 2_1^+, 4_1^+, 6_1^+, 8_1^+ states (bands) are compared with point-proton transition densities (solid curve) unfolded from the (e, e') results [20]. In the 2^+ part of the figure the contribution of the $1g_{9/2}$-$2d_{5/2}$ configuration only from work [23] is shown by the dashed curve. In the 4^+ part of the figure QRPA neutron transition density from [19] for the 4_1^+ state is presented (dotted curve). In the 8^+ part of the figure neutron transition density having proton radial form is shown by the dotted curve.

Table 3. Neutron to proton transition strenghts ratio for ^{90}Zr low-lying states.

Level J^π	E (MeV)	$B(EL)\uparrow$ (e^2b^L)	M_n/M_p [(a)]	M_n/M_p [(b)]
2_1^+	2.19	0.0656	0.66(4)	1.12(4)
3_1^-	2.75	0.0761	1.0	1.06(5)
4_1^+	3.08	0.00321	0.84(5)	0.78(12)
6_1^+	3.45	0.000231	0.62(4)	0.63
8_1^+	3.59	2.0×10^{-5}	1.58(16)	0.56

([a]) Present paper.
([b]) Dates from the work of Gazally *et al.* [3].

for high multipolarities. The obtained results M_n/M_p for multipolarity L are presented in table 3.

The surface lobes in the extracted neutron transition densities for the 2^+–6^+ states are lower in absolute value than those in the proton densities. That is why the ratio of the transition strengths M_n/M_p is smaller than a value of 1.0 (see table 3). A shifting of the surface lobes is observed for the 8^+ level. It also has a smaller amplitude than the proton one but by contrast with the 6_1^+ level it has additional structure. It is the tail of the experimental transition density that leads to a relatively large value of the M_n/M_p ratio in table 3 for this level. If we take the neutron transition density to have the same form as the proton one and adjust its amplitude to reproduce differential-cross-section normalization, we get poor agreement at large angles (see fig. 6, scaled proton transition density). Probably in this case the multistep reaction mechanism is important [19].

The proton transition densities for the 2^+-to-8^+ multiplet arise from the same dominant configuration, and thus the shape of all these densities is determined likewise by the shape of the radial wave function. The deficiency exhibited by the transition densities of the microscopic shell model calculation (valence protons) is often remedied by the coherent addition of a phenomenological core vibration amplitude (see, *e.g.*, [3,5]). It follows from Brown and Madsen [24] that the core polarization model that takes into account high-lying giant quadrupole excitation can increase the transition strength for the 2_1^+ level to the experimental one. This model also predicts a considerable contribution of neutrons in the excitation of this level, though the neutron shell is closed for ^{90}Zr. The simple schematic model of Brown and Madsen predicts a 0.67 value for the ratio M_n/M_p for the 2_1^+ level. It is seen from fig. 7 that the contributions of the neutron excitations are not weak and sometimes are even comparable to the

proton contributions. However, the shapes of both contributions are different across the board and, consequently, all the analyzed excitations are far from isoscalar.

Earlier the model-dependent neutron transition density for the 2_1^+ level was extracted [21] in the description of inelastic proton scattering at 500 MeV. However, the value obtained in [21] ($M_n/M_p = 1.47$) considerably deviates from ours. When we used the transition density of [21] in our calculations, we overestimated the differential cross-section for this level. Besides, inelastic scattering of ^{6}Li ions was used [23] to extract the ratio M_n/M_p and to test the transition densities of this level obtained from open-shell random phase approximation (RPA) calculations. The value of M_n/M_p obtained in [23] is 0.85 ± 0.10 and in a special fit it is 0.72 ± 0.10, which agrees with our value 0.66 ± 0.04.

The main difference of the experimental neutron transition density obtained in this work from the proton one for the 2_1^+ level is the existence of a negative valley of large amplitude in the vicinity of 2.5 fm. Certainly the reasons for such a difference should be traced with the help of predictions in the corresponding structure models. Thus, quite effective seem transition densities predicted by a quasiparticle RPA (QRPA) model with separable isoscalar and isovector particle-hole interactions [25]. Some encouraging results of the difference between neutron and proton densities obtained from QRPA calculations are reported in [26] for the 2_1^+ and 3_1^- states in ^{90}Zr.

We have also analyzed the results of QRPA calculations of the neutron transition density for this level represented in paper [23]. In this work, the contribution of every particle-hole configuration to the transition matrix element M_n is tabulated. The main contribution to M_n here is due to the configuration $1g_{9/2}$-$2d_{5/2}$. The neutron jumps from the closed shell $1g_{9/2}$ to the empty $2d_{5/2}$ one. The theoretical contribution to M_n of this transition ammounts to 7.58 fm^2. Only this configuration is used in our calculations of the transition density for the 2_1^+ state presented in fig. 7. Its radial dependence agrees well with the experimental neutron transition density we have obtained. The different neutron particle-hole configurations that the QRPA theory predicts considerably smooth out the negative minimum of the transition density in [23]. As a result our experimental neutron transition density for the 2_1^+ level is dominated by the transition $1g_{9/2}$-$2d_{5/2}$ only and contains contributions of other configurations with essentially smaller amplitudes than predicted by the QRPA theory.

The calculated neutron transition density for the 4_1^+ level from paper [19] is also shown in fig. 7. The experimental transition density agrees well with the calculated one. It follows that the QRPA model predicts the neutron transition density for the 4_1^+ level that agrees with the experiment.

4 Results and discussion

For the states of higher spin (6^+ and 8^+), as is seen in fig. 7, the experimental proton transition densities mainly

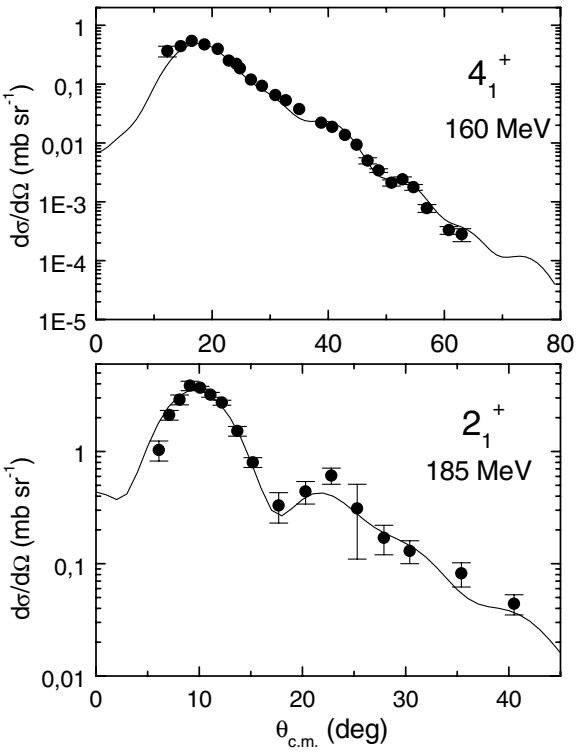

Fig. 8. Inelastic cross-sections for proton scattering from ^{90}Zr at 160 and 185 MeV. The 2_1^+ and 4_1^+ levels. The circles are the data from refs. [27,28]. The curves are microscopical folding model calculations.

outmeasure the neutron ones. This could be taken to indicate, according to [19], that these states retain some "memory" of the naive picture of them as purely proton excitations. As has already been stated, our analysis which neglected coupled-channels effects could distort the fitted neutron transition densities, first of all for the 8_1^+ state. The high 8 spin can be combined with lower spins of this multiplet in different ways. The 8_1^+ state is the weakest excitation here. So we think that if the multistep excitations are important there, they can influence the 8_1^+ level first of all. For this reason the 8^+ results shown in fig. 7 should be considered as approximate. However, it is clear that here unacceptable are both the collective interpretation and the naive interpretation of this state as a state arising from the re-coupling of two valence protons in the $1g_{9/2}$ orbit.

The most realistic seems to be the assessment [26] according to which the neutron contribution to core polarization in the 8^+ transition is substantial, leading to a neutron density of about 60% of the proton density.

5 Summary and conclusions

We have also tested the obtained neutron transition densities at different energy of incident protons. In the

experiment [27] protons of 160 MeV were used in inelastic excitation of the 4_1^+ level in ^{90}Zr. And in experiment [28] protons of 185 MeV were used in inelastic excitation of the 2_1^+ level. The calculated differential cross-sections for these levels were compared with experiments in fig. 8. The calculations were performed in the same manner as for 400 MeV. The empirical effective interaction of Kelly was used as a driven potential for this excitation [9]. As is seen from the figure, the agreement between the theory and experiment is satisfactory. This also confirms the neutron transition densities we obtained for these levels.

The authors are grateful to J. Kelly for providing us with the code LEA and to V.I. Kudriashov for the compilation of some experimental data.

References

1. P.E. Garrett, W. Younes, J.A. Becker, L.A. Bernstein *et al.*, Phys. Rev. C **68**, 024312 (2003).
2. G. Jakob, N. Benczer-Koller, J. Holden, G. Kumbartzki *et al.*, Phys. Lett. B **494**, 187 (2000).
3. M.M. Gazally, N.M. Hintz, M.A. Franey *et al.*, Phys. Rev. C **28**, 294 (1983).
4. F.T. Baker, A. Scott, M.A. Grimm *et al.*, Nucl. Phys. A **393**, 283 (1983).
5. L. Lee, T.E. Drake, S.S.M. Wong *et al.*, J. Phys. G **15**, L91 (1989).
6. A.V. Plavko, M.S. Onegin, O.A. Ponkratenko, Bull. Russ. Acad. Sci., Phys. Ser. **50**, No. 5, 117 (1986).
7. M.A. Khandaker, J.J. Kelly, P. Boberg *et al.*, Phys. Rev. C **44**, 1978 (1991).
8. A. Plavko, M. Onegin, V. Kudriashov *et al.*, AIP Conf. Proc., edited by E.J. Stephenson, S.E. Vigdor, **339**, 551 (AIP, New York, 1995).
9. J.J. Kelly, Phys. Rev. C **39**, 2120 (1989).
10. J.J. Kelly, *Computer program LEA*, unpublished, private communication.
11. L. Ray, Phys. Rev. C **41**, 2816 (1990).
12. J.J. Kelly, A.E. Feldman, B.S. Flanders, H. Seifert *et al.*, Phys. Rev. C **43**, 1272 (1991).
13. M.A. Franey, W.G. Love, Phys. Rev. C **31**, 488 (1985).
14. W.G. Love, M.A. Franey, Phys. Rev. C **24**, 1073 (1981).
15. J.J. Kelly, P. Boberg, A.E. Feldman, B.S. Flanders *et al.*, Phys. Rev. C **44**, 2602 (1991).
16. L. Lee, T.E. Drake, S.S.M. Wong, D. Frekers *et al.*, Phys. Lett. B **205**, 219 (1988).
17. L. Lee, PhD Thesis, University of Toronto (1988).
18. L. Ray, W.R. Coker, G.W. Hoffman, Phys. Rev. C **18**, 2641 (1978).
19. D.J. Horen, G.R. Satchler, S.A. Fayans, E.L. Trykov, Nucl. Phys. A **600**, 193 (1996).
20. J. Heisenberg, J. Dawson, T. Milliman *et al.*, Phys. Rev. C **29**, 97 (1984).
21. M.L. Bartlett, G.W. Hoffman, L. Ray, Phys. Rev. C **35**, 2185 (1987).
22. J.J. Kelly, B.S. Flanders, F.W. Hersman *et al.*, Phys. Rev. C **47**, 2146 (1993).
23. D.J. Horen, R.L. Auble, J. Gomez del Campo, G.R. Satchler *et al.*, Phys. Rev. C **47**, 629 (1993).
24. V.R. Brown, V.A. Madsen, Phys. Rev. C **11**, 1298 (1975).
25. V.R. Brown, J.A. Carr, V.A. Madsen, F. Petrovich, Phys. Rev. C **37**, 1537 (1988).
26. J. Heisenberg, *Nuclear Structure 1985. Proceedings of the Niels Bohr Centennial Conference* (North-Holland, Amsterdam, Oxford, New York, Tokyo, 1985) p. 229.
27. A. Scott, F.T. Baker, M.A. Grimm, J.H. Jonson *et al.*, Phys. Rev. Lett. **45**, 1315 (1980).
28. E. Hagberg, A. Ingemarsson, B. Sundqvist, Phys. Scr. **3**, 245 (1971).